Tunable UWB Metasurface Absorber for Smart City Compatible IoT Applications

Naveen Kumar Maurya[1], Sadhana Kumari[2], Prakash Pareek[1(✉)], Jayanta Ghosh[3], and Manuel J. Cabral S. Reis[4]

[1] Department of Electronics and Communication Engineering, Vishnu Institute of Technology, Bhimavaram 534202, Andhra Pradesh, India
prakash.p@vishnu.edu.in
[2] Department of Electronics and Communication Engineering, BMS College of Engineering, Bengaluru 560019, Karnataka, India
[3] Department of Electronics and Communication Engineering, National Institute of Technology, Patna 800005, Bihar, India
[4] Engineering Department, UTAD/IEETA, 5001-801 Vila Real, Portugal

Abstract. This work presents an ultra-wideband tunable graphene-based metasurface absorber for the terahertz (THz) gap region of the electromagnetic (EM) spectrum. The proposed absorber provides an absorption bandwidth (BW) of 7.8 THz (fractional BW = 195%) with absorptivity $A(f) \geq 90\%$, i.e., from 0.1 to 7.9 THz. The impedance matching between free space and the absorber's surface has been achieved by engraving different shapes of slots on the top graphene layer. The working principle behind the UWB absorption mechanism has also been studied with the help of parametric studies and field plots. The thickness of the metasurface is only 2 µm, i.e., $\lambda_g/958.3$, where λ_g has been computed at 0.1 THz, thus, maintaining the ultra-thin nature required for the metasurface design in the THz regime. The absorber's periodicity is also quite less, i.e., 6 µm ($\lambda_g/319.43$), which is sufficient to achieve an effective homogeneity condition. The four-fold symmetry in the design makes the structure polarization insensitive to the incoming plane wave. The metasurface also works well for a wide incidence angle (θ) under both transverse electric (TE) and transverse magnetic (TM) polarizations. The $A(f) \geq 80\%$ has been achieved for θ up to 45°. In addition, the absorber provides full-width at half-maxima (FWHM) BW in the complete frequency range, i.e., from 0.1 to 7.9 THz. Hence, the proposed metasurface absorber is found suitable for suppressing/absorbing unwanted electromagnetic radiation in a close indoor environment for smart city-enabled Internet of Things (IoT) applications.

Keywords: Metasurface · Graphene · Ultra-wideband · Terahertz

P. Pareek et al. (Eds.): IC4S 2023, LNICST 537, pp. 231–240, 2024.
https://doi.org/10.1007/978-3-031-48891-7_20

1 Introduction

A recent worldwide survey by United Nations revealed that a major chunk of the world's population will migrate to cities in the coming years [1]. Due to the exponential increase in the population of cities triggered by massive urbanization, city administrators are looking for viable solutions that effectively monitor the citizen to enhance their living standards. In this context, the smart city emerged as the potential key to quenching this quest. The smart city ecosystem allows the city administration to effectively and precisely implement various aspects of the city, like security, transportation, cleaning and sanitation, etc., through proper monitoring and sensing [2]. Indeed, the functioning of smart city applications relies on gathering data from various devices/sensors wirelessly, analyzing these data, implementing intelligent control measures, and securely disseminating information [3].

Hence, to tackle smart cities' complex and diverse challenges, the internet is crucial in facilitating communication, sharing and processing information, transferring and analyzing data, and enabling distributed computing. The emergence of the Internet of Things (IoT) and the widespread integration of web technologies for cloud computing in urban settings have demonstrated the effectiveness of Internet-based solutions in effectively addressing societal issues [4]. In order to realize this vision, the next generation of IoT devices must be created with the capability to operate autonomously through wireless medium [5] and support numerous wireless standards [6,7]. Additionally, precise sensing plays a critical role in enabling autonomy in smart cities and researchers worldwide have attempted various devices and technologies to improve the sensitivities of IoT sensors [8].

Metamaterials/metasurfaces are unique materials that possess properties that are not naturally occurring and are composed of resonators arranged in a uniform pattern on a dielectric substrate [9]. Interestingly, metamaterials/metasurfaces exhibit diverse properties, including the ability to selectively absorb specific frequencies [10–13] or detect even the slightest variations in specific parameters [12,14–16]. Thus, metasurfaces hold significant potential for utilization in various smart city compatible IoT applications due to their distinctive characteristics such as absorbers, modulators, sensors, switches, etc. [9,12,14,15,17]. At the same time, these artificially engineered materials have the capacity to absorb undesired frequencies, which is crucial to avoid cross-talk between wireless sensor nodes and provide end users with the best performance. These intriguing characteristics make them valuable for supporting IoT technology in challenging conditions, primarily through their precise sensing and absorption applications [18]. Since the population is increasing at an astonishing rate [1], the demand for higher data rates will also be going to increase exponentially. This motivates the researchers to shift towards the terahertz (THz) range of electromagnetic (EM) spectrum due to the availability of ultra-wideband (UWB) frequency spectrum and non-ionizing nature of THz radiation [19]. Hence, the future smart city compatible IoT applications will incorporate THz technology for UWB communication [20,21].

This work focuses on the design and analysis of frequency tunable metasurface for absorption over an UWB band in the THz regime. The tunable frequency response enables the proposed absorber to be used as a sensor, modulator, and switch apart from its usage as an absorber. The rest of the paper has been organized as follows: The design procedure has been presented in Sect. 2. Section 3 focus on the results and discussions. Finally, Sect. 4 concludes this work.

2 Metasurface Design

In the THz regime, graphene-based designs have gotten tremendous attention due to their ability to generate plasmonic resonances by exciting surface plasmon polaritons (SPPs) [9,22–24]. Interestingly, these resonances could be made frequency reconfigurable by varying complex surface conductivity of the graphene (σ_{graphene}) defined by Eq. 1, which is the summation of intra-band (σ_{intra}) and inter-band (σ_{inter}) conductivities given by Eq. 2 and 3, respectively [25]. In the THz gap region of the EM spectrum (0.1–10 THz), the contribution of σ_{inter} could be ignored [9,22]. Therefore, σ_{graphene} could be independently represented by σ_{intra}. As a result, by varying chemical potential (μ_c) in Eq. 2, σ_{graphene} could be varied. Thereby imparting plasmonic resonances reconfigurable frequency characteristics in the graphene-based devices.

$$\sigma_{\text{graphene}} = \sigma_{\text{intra}} + \sigma_{\text{inter}} \tag{1}$$

$$\sigma_{\text{intra}} = -j\frac{e^2 k_B T}{\pi\hbar^2(\omega - j\Gamma)}\left[\frac{\mu_c}{k_B T} + 2\ln(e^{-\mu_c/k_B T} + 1)\right] \tag{2}$$

$$\sigma_{\text{inter}} = \frac{-je^2}{4\pi\hbar}\ln\left(\frac{2|\mu_c| - (\omega - j\Gamma)\hbar}{2|\mu_c| + (\omega - j\Gamma)\hbar}\right) \tag{3}$$

The schematic diagram of the proposed graphene-based tunable UWB metasurface absorber is shown in Fig. 1a and the corresponding reflection and absorption curves have been depicted in Fig. 1b. The structure of the unit cell comprises of SiO_2 ($\epsilon_r = 3.9$ and $\tan\delta = 0.0006$) substrate backed by continuous monolayer graphene (MLG) sheet having a thickness of 0.335 nm. The top surface of the unit cell has also been designed using a 0.335 nm thick MLG sheet. Since the SiO_2 substrate is backed by the MLG sheet having thickness greater than the skin depth, the transmission coefficient ($|S_{21}|$) becomes zero and the absorptivity ($A(f)$) defined by Eq. 4 depends only on the reflection coefficient ($|S_{11}|$) represented by Eq. 5. Hence, in this work, the UWB absorption response has been obtained by achieving impedance matching between the absorber's top surface and free space.

Interestingly, while designing the metasurface unit cell in this work, the reflections at the interface between the absorber's surface and free space have been reduced by incorporating slots of different shapes (viz. square loop and circular) and sizes on the top of the MLG sheet, as shown in Fig. 1a. It is worthy to mention here that the square-shaped slots with two different sizes have been used here

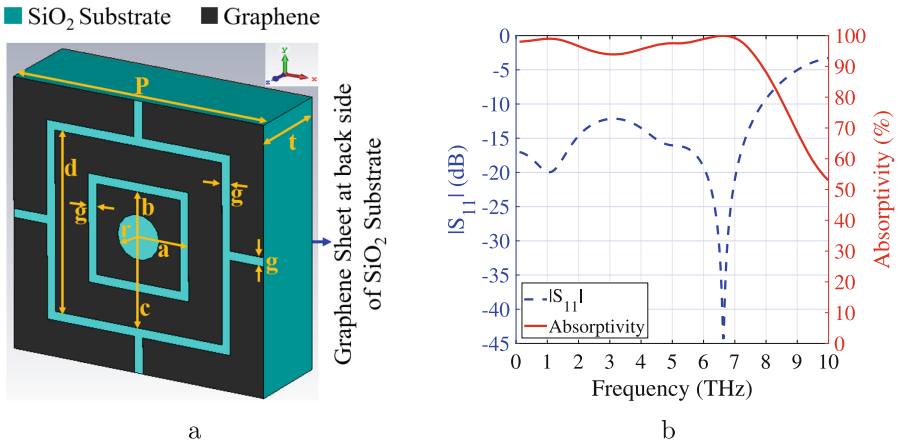

Fig. 1. (a) Perspective view of the proposed UWB absorber, $P = 6$, $t = 2$, $a = 1.2$, $b = 1$, $c = 2$, $d = 4$, $g = 0.2$, $r = 0.5$ (unit:μm) and (b) $|S_{11}|$ and absorptivity.

to excite two distinct plasmonic resonances. The larger square slot resonates at 1.06 THz, whereas the smaller square loop slot resonates at 3.14 THz. In addition, the central circular slot resonates at 6.63 THz. Subsequently, the three distinct plasmonic resonances generated by square and circular slots have been combined together to provide a UWB absorptivity response. The proposed UWB absorber covers the THz frequency spectrum from 0.1 to 7.9 THz with $A(f) \geq 90\%$, which corresponds to 195% fractional bandwidth (FBW) as shown in Fig. 1b. The periodicity and thickness of the metasurface are $\lambda_g/319.43$ and $\lambda_g/958.3$, respectively, where λ_g is the guided wavelength computed at 0.1 THz, thus, satisfying both the effective homogeneity condition and the ultra-thin nature required for designing a metasurface absorber in the THz regime.

$$A(f) = 1 - |S_{11}|^2 - |S_{21}|^2 \tag{4}$$

$$A(f) = 1 - |S_{11}|^2 \tag{5}$$

3 Results and Discussions

To have a better understanding regarding the excitation of localized SPP (LSPP) wave, generation of resonant modes and loss mechanism taking place inside the absorber structure, magnitude E-field and magnitude H-field have been numerically computed using CST Microwave Studio in the xy-plane as shown in Figs. 2 and 3, respectively. The |E|-field distribution depicted in Fig. 2a clearly shows that the outer square slot ring is mostly excited at 1.06 THz while the inner square slot ring and central circular slot remain unenergized. This confirms the electric excitation of the metasurface absorber by the incoming plane wave, which

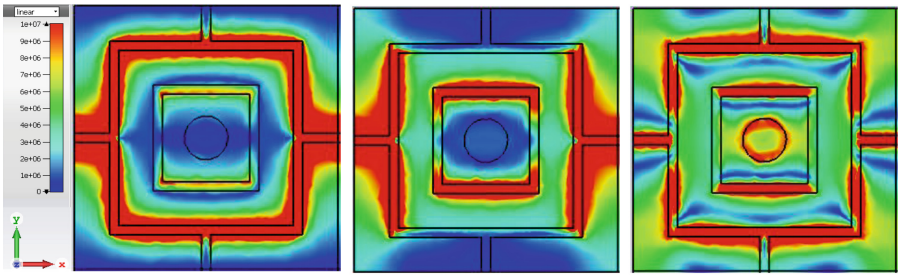

a b c

Fig. 2. |E|-field density at: (a) 1.06 THz, (b) 3.14 THz, and (c) 6.63 THz in xy-plane.

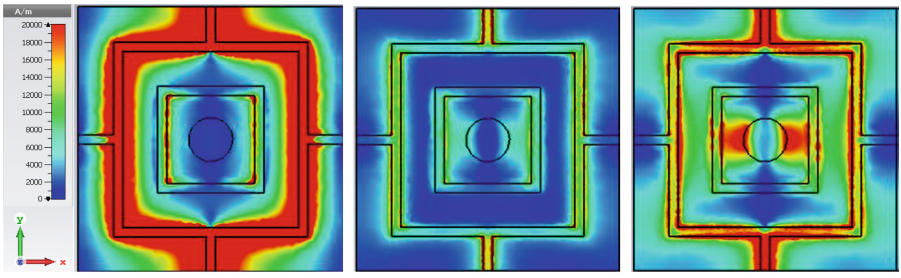

a b c

Fig. 3. |H|-field density at: (a) 1.06 THz, (b) 3.14 THz, and (c) 6.63 THz in xy-plane.

leads to the generation of the LSPP wave at the interface of the graphene and dielectric substrate near the vicinity of the outer square ring. The LSPP wave is non-propagative in nature and mostly oscillates at its position. This causes energy localization and thereby leads to losses in the form of conductor loss induced by graphene and dielectric loss induced by the SiO_2 substrate. It is worthy to mention here that the perimeter of the outer square ring is more compared to the inner square ring and circular slot. As a result, the outer square ring generates plasmonic resonance at the lowest operating frequency, i.e., at 1.06 THz. The |H|-field density has also been computed at 1.06 THz to analyze the response of the proposed metasurface with respect to the H-field vector of the incident plane wave as shown in Fig. 3a. From Fig. 3a, it is evident that the induced H-field is mostly concentrated inside the outer square loop and it is orthogonal to the |E|-field distribution shown in Fig. 2a. Hence, perfect absorption takes place at 1.06 THz with a sharp dip in $|S_{11}|$ characteristics (see Fig. 1b) through proper electromagnetic excitation of the metasurface absorber.

Similarly, the |E|-field and |H|-field densities have been computed at 3.14 THz as shown in Figs. 2b and 3b, respectively. The field plots reveal that the inner square ring is excited in its fundamental mode, i.e., one wavelength loop mode

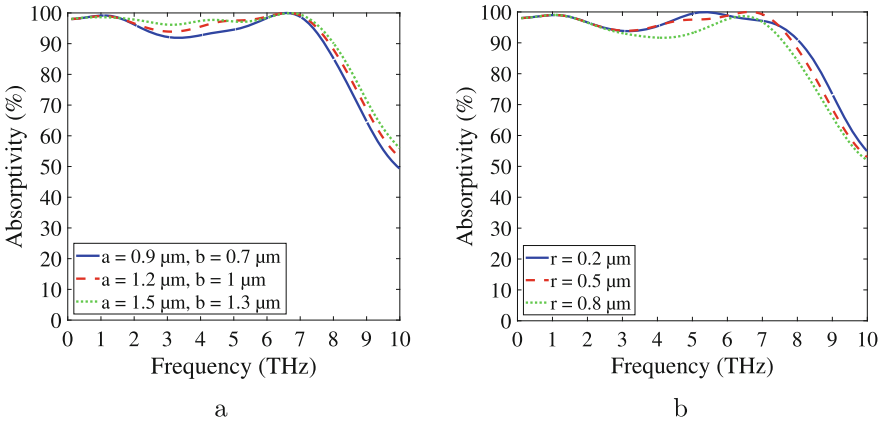

Fig. 4. Parametric study for the variation in: (a) parameters a and b, simultaneously such that $(a\text{-}b) = g$ is constant at 0.2 μm and (b) r.

[22], which is responsible for the absorption mechanism at 3.14 THz. In addition, at 3.14 THz, the outer square ring has also been excited in its higher-order mode. As a result, two distinct resonances generated by the inner square ring and outer square ring combined together to provide a UWB absorptivity response. Finally, a strong electromagnetic excitation of the central circular slot at 6.63 THz shown in Figs. 2c and 3c leads to the sharp dip in $|S_{11}|$ characteristics as shown in Fig. 1b. The strong confinement of the electric and magnetic fields near the central circular slot clearly indicates the generation of the LSPP wave, which is responsible for the absorption of the EM wave towards the upper side of the UWB absorption band. Here also, the outer and inner square rings are excited in their higher-order loop modes, which justifies the recombination of different modes to provide a UWB absorption response.

The observations made above by analyzing the |E|-field and |H|-field densities have been further verified with the help of the parametric study of the design variables as shown in Fig. 4. Due to brevity, the effect of variation in the perimeter of the outer square ring has been ignored. This is because, at 1.06 THz, only the outer square loop is energized and the other two slots remain unexcited, as shown in Figs. 2a and 3a, which clearly show that at 1.06 THz, absorption is taking place due to the excitation of the outer square loop only. In the first parametric study, parameters a and b have been varied simultaneously such that a-b, i.e., g (see Fig. 1a) is always constant at 0.2 μm while keeping all other parameters unchanged as shown in Fig. 4a. With an increase in parameters a and b, the perimeter of the inner square ring increases. As a result, the level of absorption near the center of the absorption band (i.e., around 3.14 THz) gets modulated without any change in the absorption peaks at 1.06 THz and 6.63 THz as shown in Fig. 4a. The same conclusion has been drawn using the |E|-field and |H|-field density shown in Figs. 2b and 3b, respectively, where we have claimed that the inner square ring is mainly responsible for absorption near 3.14 THz. In the next

study, the radius of the central circular slot (r) has been varied from 0.2 to 0.8 µm, as shown in Fig. 4b. With an increase in r, it is evident that the absorption curve is getting changed mostly near the 6.63 THz, which again justifies our claim that r is responsible for absorption near the higher side of the absorption band.

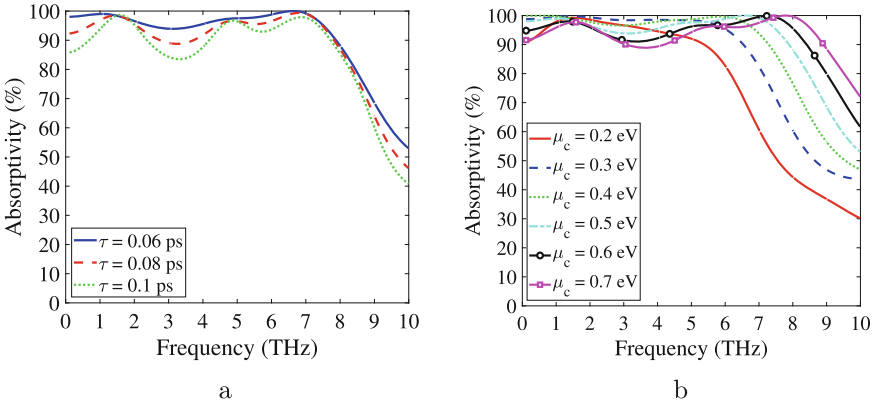

Fig. 5. Parametric study for the variaton in: (a) τ and (b) μ_c of the graphene.

The effect of graphene's electrical parameters viz. τ and μ_c on the $A(f)$ has also been analyzed using a parametric study as shown in Fig. 5. For the higher value of τ, the absorption coefficient changes from UWB to the multiband nature. Hence, in this work a lower value of τ, i.e., 0.06 ps, has been considered to obtain an ultra-wideband response over a multiband response. To test the tunable frequency characteristics of the proposed graphene-based metasurface absorber, the complex surface conductivity of graphene has been varied by changing μ_c as shown in Fig. 5b. From Fig. 5b, it is evident that with an increase in the value of μ_c, $A(f)$ response is clearly showing frequency tunability with a blue shift in absorption curves. Moreover, absorption BW also increases for higher values of μ_c as shown in Fig. 5b. For $\mu_c = 0.5$ eV, the absorber provides BW of 7.8 THz with $A(f) \geq 94\%$. With a further increment in μ_c beyond 0.5 eV, the absorption BW is increasing but at the cost of a decrease in the level of absorptivity. Hence, $\mu_c = 0.5$ eV has been selected in this work.

The orientation of the E-field vector and the angle of incidence of incoming plane waves can severely affect the absorption coefficient of a metasurface absorber. To examine this, the effect of the polarization angle (ϕ) and incidence angle (θ) has been studied, as shown in Fig. 6. Figure 6a shows that with the change in ϕ from 0° to 45°, the absorption coefficient remains unchanged, which confirms the polarization insensitivity of the proposed absorber. For the perfect absorption of EM waves in indoor wireless environments for massive IoT applications, polarization insensitivity is one of the most crucial factors. In an indoor wireless environment, multiple reflections and scattering of EM waves

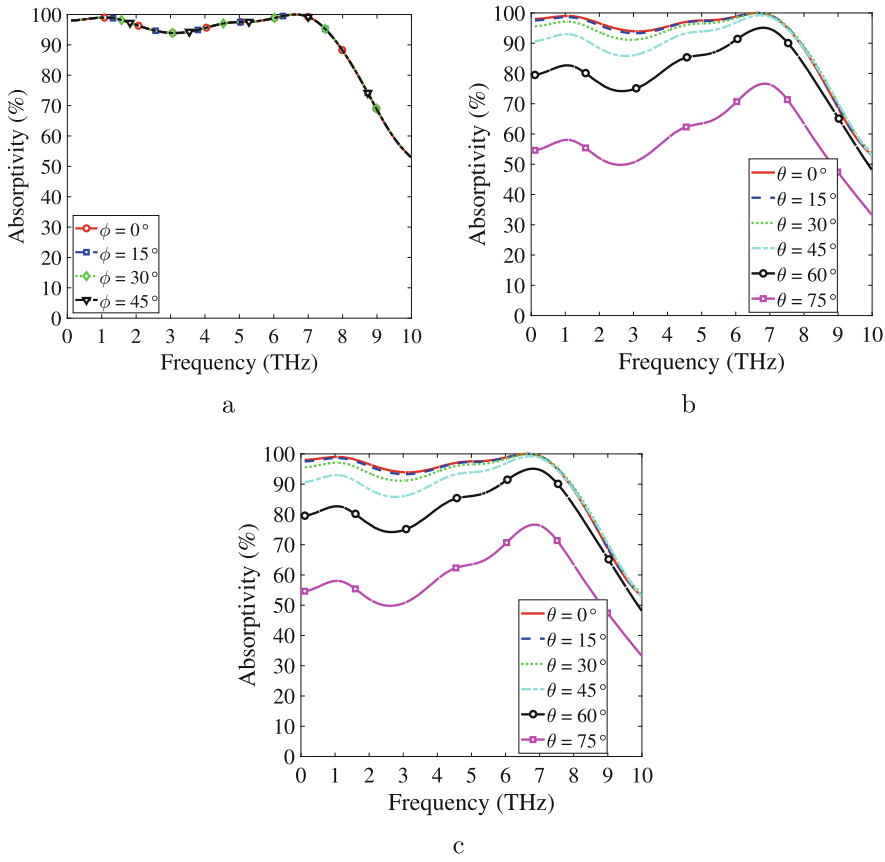

Fig. 6. (a) $A(f)$ for different polarization angles (ϕ). $A(f)$ for different incidence angles (θ) under: (b) TM polarization ($\phi = 0°$) and (c) TE polarization ($\phi = 90°$).

occur, often changing the polarization angle of the incident plane wave. Therefore, making absorber polarization insensitive can helps to absorb EM waves having different polarization angles as well. Similarly, the effect of θ under both transverse magnetic (TM) and transverse electric (TE) has also been analyzed, as shown in Fig. 6b and c. It is found that the proposed absorber provides $A(f) \geq 80\%$ up to $\theta = 45°$. At the same time, the proposed absorber also covers the BW from 0.1 to 7.9 THz with $A(f) \geq 50\%$, thus, providing very wide full-width half-maxima (FWHM) bandwidth, which is very much required for massive IoT applications in multipath-rich wireless environment taking place in closed indoor environment.

The efficacy of the proposed work has been brought to the attention by comparing it with current state-of-the-art designs present in the literature as shown in Table 1. The proposed work provides the highest absorption BW of 195%, which is far better than the others, as shown in Table 1. At the same

time, the thickness and periodicity of the proposed design are also quite less, as shown in Table 1. Hence, the proposed metasurface could be one of the good solutions for absorber application over ultra-wideband in the THz regime.

Table 1. Comparison Study

Reference	Freq Range (THz) For A(f) $\geq$ 90%	Fractional BW (%)	Thickness	Periodicity	Design Configuration
[10]	2.06–11.8	140.86	$\lambda_0/55.9$	$\lambda_0/21.7$	Graphene-Dielectric-Graphene
[11]	1.07–2.88	91.64	$\lambda_0/11$	$\lambda_0/14$	Graphene-Dielectric-Gold
[12]	4–8	67	$\lambda_0/8.39$	$\lambda_0/9.38$	Hybrid-Dielectric-Gold
[13]	2.2–4.6	70.59	$\lambda_0 11.36$	$\lambda_0/13.64$	Graphene-Dielectric-Gold
This Work	0.1–7.9	195	$\lambda_0/1500$	$\lambda_0/500$	Graphene-Dielectric-Graphene

4 Conclusions

This work presents a frequency-reconfigurable UWB metasurface absorber for the THz regime. The tunability in the design has been achieved by using graphene as a design material. Interestingly, the tunable absorption characteristic also allows the proposed solution to be used for sensing and switching applications. The structural symmetry in the design makes the metasurface independent from the polarization of the incident plane wave. In addition, the proposed absorber also provides a good absorption response under a wide incident angle over the UWB band. Hence, the designed tunable metasurface absorber could be used in smart city scenarios to suppress unwanted interference over the UWB band that takes place in indoor wireless environments, particularly for IoT applications.

References

1. Da Silva, I.N., Flauzino, R.A.: Smart Cities Technologies, 1st edn. Intechopen, London (2016)
2. Pareek, P., Maurya, N.K., Singh, L., Gupta, N., Reis, M.J.C.S.: Study of smart city compatible monolithic quantum well photodetector. In: Gupta, N., Pareek, P., Reis, M. (eds.) IC4S 2022. LNCS, SITE, vol. 472, pp. 215–224. Springer, Cham (2023). https://doi.org/10.1007/978-3-031-28975-0_18
3. Iqbal, A., Olariu, S.: A survey of enabling technologies for smart communities. Smart Cities **4**(1), 54–77 (2020)
4. Bellini, P., Pantaleo, G.: Special issue on the internet of things (IoT) in smart cities (2023)
5. Rafiq, I., Mahmood, A., Razzaq, S., Jafri, S.H.M., Aziz, I.: IoT applications and challenges in smart cities and services. J. Eng. **2023**(4), e12262 (2023)
6. Maurya, N.K., Bhattacharya, R.: Design of compact dual-polarized multiband MIMO antenna using near-field for IoT. AEU-Int. J. Electron. Commun. **117**, 153091 (2020)

7. Maurya, N.K., Bhattacharya, R.: CPW-fed dual-band compact Yagi-type pattern diversity antenna for LTE and WiFi. Prog. Electromagn. Res. C **107**, 183–201 (2021)
8. Sisinni, E., Saifullah, A., Han, S., Jennehag, U., Gidlund, M.: Industrial internet of things: challenges, opportunities, and directions. IEEE Trans. Industr. Inf. **14**(11), 4724–4734 (2018)
9. Maurya, N.K., Ghosh, J., Sumithra, P.: Design of graphene-based tunable ultra-thin UWB metasurface for terahertz regime. Optik, 170753 (2023)
10. Ghosh, S.K., Das, S., Bhattacharyya, S.: Graphene based metasurface with near unity broadband absorption in the terahertz gap. Int. J. RF Microwave Comput. Aided Eng. **30**(12), e22436 (2020)
11. Yadav, V.S., Kaushik, B.K., Patnaik, A.: Broadband THz absorber for large inclination angle TE and TM waves. IEEE Photonics J. **13**(5), 1–7 (2021)
12. Lv, Y., Liu, W., Tian, J., Yang, R.: Broadband terahertz metamaterial absorber and modulator based on hybrid graphene-gold pattern. Physica E **140**, 115142 (2022)
13. Zakir, S., et al.: Polarization-insensitive, broadband, and tunable terahertz absorber using slotted-square graphene meta-rings. IEEE Photonics J. **15**(1), 1–8 (2022)
14. Shen, H., et al.: Multi-band plasmonic absorber based on hybrid metal-graphene metasurface for refractive index sensing application. Results Phys. **23**, 104020 (2021)
15. Khan, M.S., Giri, P., Varshney, G.: Generating multiple resonances in ultrathin silicon for highly selective THz biosensing. Physica Scripta **97**(8), 085009 (2022)
16. Shalini, V.B.: A polarization insensitive miniaturized pentaband metamaterial THz absorber for material sensing applications. Opt. Quant. Electron. **53**, 1–14 (2021)
17. Shabani, M., Karimi, G.: Compact single-band and multiband terahertz plasmonic absorbers using hybrid graphene-metal resonators with switching and modulation capability. Optik, 171010 (2023)
18. Amiri, M., Tofigh, F., Shariati, N., Lipman, J., Abolhasan, M.: Review on metamaterial perfect absorbers and their applications to IoT. IEEE Internet Things J. **8**(6), 4105–4131 (2020)
19. Tonouchi, M.: Cutting-edge terahertz technology. Nat. Photonics **1**(2), 97–105 (2007)
20. Farooq, M.S., Nadir, R.M., Rustam, F., Hur, S., Park, Y., Ashraf, I.: Nested bee hive: a conceptual multilayer architecture for 6G in futuristic sustainable smart cities. Sensors **22**(16), 5950 (2022)
21. Niu, M.: Intelligent Electronics and Circuits: Terahertz, Its, and Beyond, 1st edn. Intechopen, London (2022)
22. Maurya, N.K., Kumari, S., Pareek, P., Singh, L.: Graphene-based frequency agile isolation enhancement mechanism for MIMO antenna in terahertz regime. Nano Commun. Netw. 100436 (2023)
23. Ram, G.C., Sambaiah, P., Yuvaraj, S., Kartikeyan, M.: Graphene based tunable bandpass filter for terahertz spectroscopy of polymers. Optik **268**, 169792 (2022)
24. Ram, G.C., Sambaiah, P., Yuvaraj, S., Kartikeyan, M.: Tunable bandstop filter using graphene in terahertz frequency band. AEU-Int. J. Electron. Commun. **144**, 154047 (2022)
25. Neto, A.C., Guinea, F., Peres, N.M., Novoselov, K.S., Geim, A.K.: The electronic properties of graphene. Rev. Mod. Phys. **81**(1), 109 (2009)